THE ASTROPHYSICAL JOURNAL, 273:688–696, 1983 October 15

THE X-RAY LOBES OF SS 433

M. G. WATSON AND R. WILLINGALE
X-Ray Astronomy Group, Physics Department, University of Leicester
AND
J. E. GRINDLAY AND F. D. SEWARD
Harvard-Smithsonian Center for Astrophysics
Received 1983 February 3; accepted 1983 March 30

ABSTRACT

We report observations of SS 433 and the surrounding region made with the imaging detectors on the *Einstein Observatory*. The observations are used to map a $\sim 2° \times 1°$ region containing W50 centered on SS 433. The results show two bright, diffuse lobes of X-ray emission symmetrically displaced E and W of SS 433, aligned along the long axis of W50. Each lobe is visible between $\sim 15'$ and $40'$ from SS 433, with emission peaking at $\sim 35'$. The bulk of the emission from each lobe is confined to a region subtending an angle of $\sim 30°$ at the central object. The soft X-ray luminosity of each lobe is $\sim 6 \times 10^{34}$ ergs s^{-1}, and X-ray spectra indicate that the diffuse emission is considerably softer than SS 433 itself. The properties and origin of these lobes, and their relationship to W50, are discussed in the context of the kinematic beam model for SS 433.

Subject headings: stars: individual — X-rays: binaries

I. INTRODUCTION

The basic observational details of the extraordinary emission-line object SS 433 are now well established after more than 3 years of intensive study by both optical and radio astronomers (e.g., Margon 1981, 1982). The principal feature which makes SS 433 so unusual is the presence of intense optical emission lines which display periodically varying redshifts and blueshifts with full amplitude $\sim 80{,}000$ km s^{-1}. A model has emerged which goes a long way toward explaining the enormous Doppler shifts of these lines: the "kinematic model" (e.g., Abell and Margon 1979). In this model two relativistic jets of matter are ejected from SS 433 at $0.26c$ in opposite directions and precess on a cone of 20° half-angle with a 164 day period, the entire system being inclined at 80° to the line of sight. Strong support for this model has recently been provided by the VLA observations of Hjellming and Johnston (1981) which demonstrate that changes in the arc second radio structure of SS 433 on time scales of tens of days can be correlated with expected space motions of the precessing jets. The VLA data, combined with the kinematic model parameters, also allow the determination of the position angle of the jet axis on the sky (i.e., P.A. $\approx 100°$) and give a good estimate of the distance to SS 433 (5.5 ± 1 kpc). Spectroscopic observations of the "stationary" emission line system in SS 433 yield a further important finding—a 13 day modulation which is probably the binary period of the system (Crampton, Cowley, and Hutchings 1980).

SS 433 is also of particular interest because of its location near the centre of the radio shell of W50, a possible galactic supernova remnant (Velusamy and Kundu 1974; Clark, Caswell, and Green 1975; Geldzahler, Pauls, and Salter 1980). Many authors have suggested a physical association between SS 433 and W50 (e.g., Begelman *et al.* 1980; Zealey, Dopita, and Malin 1980), both because of this positional coincidence, and, more compelling, because of the asymmetric ansae in W50 which are aligned along the same position angle (i.e., $\sim 100°$) as that determined for the relativistic jets by the VLA observations.

This work extends the original paper by Seward *et al.* (1980) which was based on only part of the data now available.

II. OBSERVATIONS

The region surrounding SS 433 was mapped with the *Einstein Observatory* Imaging Proportional Counter in three partially overlapping observations with similar long exposure times. Each observation gives an X-ray image in a soft X-ray band (nominally 0.5–4.5 keV) covering a square field of width 1° with arcminute resolution. Details of the *Einstein Observatory* and scientific instruments are given in Giacconi *et al.* (1979). One observation was centered on SS 433; the other two were offset by $30'$–$40'$ east and west, respectively, to give on-axis coverage of the extended emission visible at the edges of the central image (cf. the original discovery of the lobes:

TABLE 1

SUMMARY OF EINSTEIN OBSERVATIONS OF SS 433

OBSERVATION	DATE	POINTING AXIS (1950.0) R.A.	Decl.	EXPOSURE TIME (s)
4623 (IPC)	1979 Oct 5–20	$19^h09^m20^s$	+4°54′00″	17099
5282 (IPC)	1979 Apr 22–24	19 06 00	+5 00 00	15781
10193 (IPC)	1980 Oct 8	19 11 00	+4 50 30	15999

Seward *et al.* 1980). Details of the observations are given in Table 1.

The three IPC observations have been merged to give a composite X-ray image which is shown in Figure 1. In the merging procedure the individual images were restricted to the same energy range, taking into account the different detector gains, and were normalized to the same exposure time and corrected for telescope vignetting expected at 1.5 keV (see § III). The final image was also corrected for the enhanced exposure where the component images overlap and has been smoothed by cross-correlation with a Gaussian of width $\sigma = 45''$. Because the effective gain and apparent background varies between each observation, the uncertainties in the intensity normalisation of the composite image are of the order 10%.

As Figure 1 clearly shows, in addition to the point source coincident with SS 433, there are also two bright, diffuse regions of emission symmetrically displaced approximately east and west of SS 433. These are the X-ray "lobes".

III. ANALYSIS AND RESULTS

We have used the IPC data to investigate the X-ray flux, spectrum, and spatial distribution of the emission from the lobes. Detailed analysis of the properties of SS 433 itself is not presented, since the X-ray spectrum and variability of SS 433 are the subject of a separate paper (Grindlay *et al.* 1983). We note however that comparison of the radial profile of the counts from SS 433 with that expected for a point source shows that it is unresolved in the IPC data: any source extent must be on angular scales $< 1'$.

a) Morphology of the Lobes

It is evident from the images shown in Figure 1 that the lobes of X-ray emission are crudely mirror-symmetric about the central source and have an elongated, fan-shaped morphology. For this reason (and anticipating the physical connection between the lobes and SS 433 discussed later), we have chosen to examine the morphology of the lobes using radial and azimuthal distributions of X-ray surface brightness in a polar coordinate system centered on SS 433. Figure 2 shows the radial brightness distributions for both E and W lobes, and Figure 3 the azimuthal distribution for the E lobe (the W lobe is very similar). Because the lobe emission spans the image boundaries, the radial profiles have been extracted from the composite image (Fig. 1) rather than on the component images. This leads to some uncertainties in the profiles since the component images have somewhat different detector gains and background levels as is discussed in § II.

Table 2 summarizes the morphological parameters derived from the radial and azimuthal profiles. Comparison of the parameters given (and the profiles themselves) demonstrates the close similarity between the E and W lobe, although there is also significant structure on arcminute scales in each lobe which is clearly not mirrored in the other lobe. At an assumed distance of 5.5 kpc, lobe emission is detected at projected distances ranging from ~ 25 to 70 pc from SS 433, and the lobes have a FWHM width of ~ 30 pc at the radius of the emission peak. Although the azimuthal distribution of the lobe surface brightness has a narrow core characterised by a FWHM of ~ 15°, broad, faint wings can also be seen extending out to full widths of at least ~ 50° (estimate limited by detectability above background). Note also that the azimuthal profile calculated for the soft energy band is significantly broader than that for the hard band. The position angles of the azimuthal maxima for E and W lobes when combined give a position angle of $99° \pm 2°$ for the axis of the X-ray lobes, very similar to the value determined from the arc second radio structure (Hjellming and Johnston 1981) and completely consistent with the position angle of the long axis of W50.

b) X-Ray Spectra, Fluxes, and Luminosities

Obtaining reliable X-ray spectra from the PHA data available from the IPC has proved rather difficult (see, e.g., Gorenstein, Harnden, and Fabricant 1981). The principal problems are the limited energy range and poor energy resolution of the IPC, together with the temporal and spatial variations in the detector gain. In the case of the lobes of SS 433, the derived spectra are also sensitive to the assumed background level and spectrum because of the relatively low surface brightness of the lobes. In the spectral analysis of the lobes we have therefore chosen to concentrate on the E lobe which is

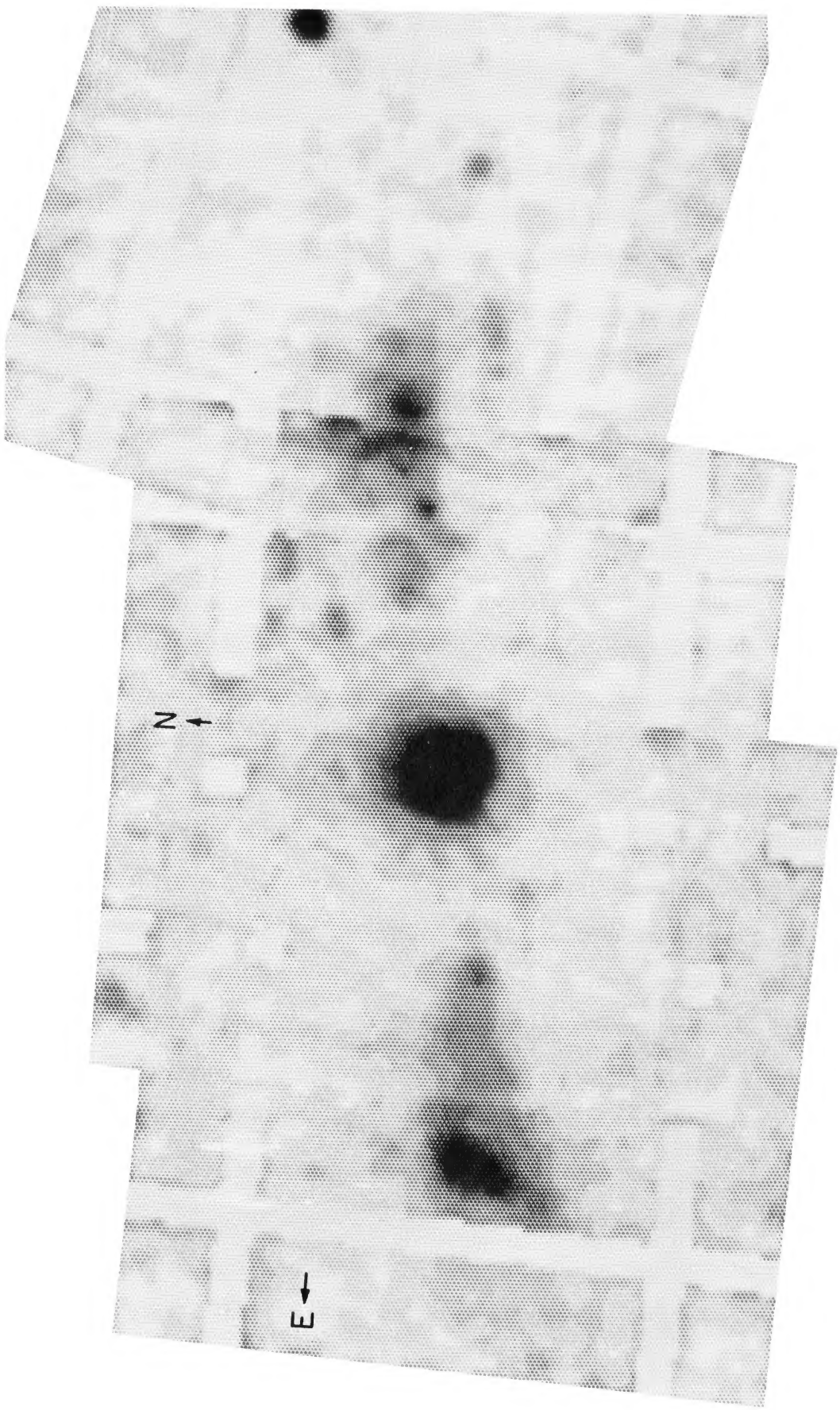

FIG. 1*a*.—IPC X-ray image of SS 433 and the surrounding region in ~ 0.7–4 keV band with 64″ pixels. The image is a composite of three separate observations, each corrected for telescope vignetting. The composite image has been smoothed with a Gaussian of width $\sigma = 45''$.

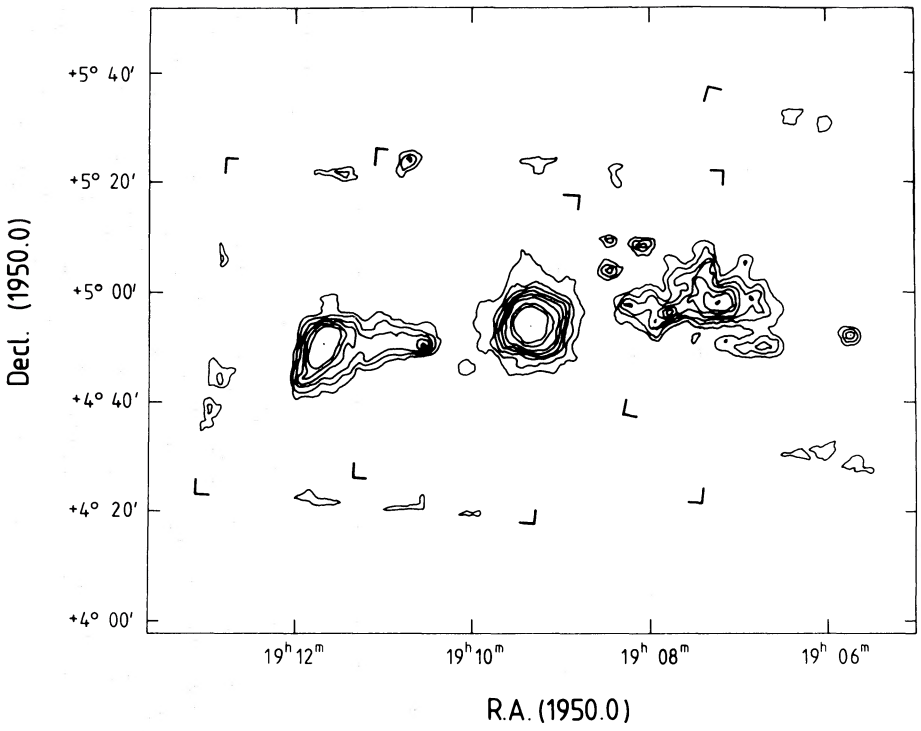

FIG. 1*b*.—Contour map version of the image shown in Fig. 1*a*. Contour levels plotted correspond to $(2.3, 2.8, 3.3, 3.9, 4.4, 4.9, 10, 15) \times 10^{-3}$ IPC counts s^{-1} arcmin^{-2}. The lowest contour corresponds to $\sim 7\ \sigma$ above background, and the interval between the first six contours to $\sim 2.5\ \sigma$. The corners of each component image are marked.

well centered in one of the three IPC images (sequence 10193) and for which we know the detector gain at the time of the observation. PHA spectra were extracted from the data for four circular regions of $\sim 4'$ radius in the brightest parts of the lobe, as shown in Figure 4. Spatial gain corrections were established using calibration data, and the background subtracted was carefully selected after comparing data from this image and a blank field with similar gain.

For each region spectral fits were made for trial input spectra corresponding to power-law and optically thin thermal forms, in each case including an absorption term of the form $\exp[-\sigma(E)N_{\rm H}]$ with the plasma temperature (or power-law index) and absorbing column density ($N_{\rm H}$) as free parameters. Because of the limited spectral capability of the IPC, the uncertainties in the best fit parameters are rather large and do not give particularly useful constraints on the physical conditions in the emission region. We can, however, use independent information to constrain the absorbing column density. Spectral fits to the *Einstein* MPC observations of SS 433 give $N_{\rm H} \sim 10^{22}$ cm^{-2} (Grindlay *et al.* 1982) in reasonable agreement with the H I column ($N_{\rm H\ I} = 8 \times 10^{21}$, quoted in Margon *et al.* 1979) and the estimated visual extinction (Margon *et al.* 1979). Assuming that the observed column density is predominantly interstellar (i.e., not intrinsic to SS 433—this is probably justified by the large dimensions inferred for the X-ray emission region in SS 433), we adopt $N_{\rm H} = 10^{22}$ cm^2 as the column density in the line of sight to the X-ray lobes. This value is consistent with all the two-parameter spectral fits to the IPC data, and of course with the column density expected at a distance of 5.5 kpc near the galactic plane.

In Table 3 we quote the results for fits to the thermal and power-law spectra with $N_{\rm H}$ fixed at 10^{22} cm^{-2}. Although the errors on the spectral parameters are still quite large, the best fit parameters for different regions are only marginally compatible with the same spectral parameters for each region. The possible trend seen corresponds to a spectral softening with increasing distance from SS 433. There is also evidence for spectral softening with increasing azimuthal angle away from the axis of the lobes (e.g., Fig. 3). Note that both thermal and power-law spectra give statistically acceptable fits to the data.

Reliable spectral fits were not possible for the image covering the W lobe (sequence 5282), but we note that the PHA data for the W lobe are completely consistent with the range of spectral parameters found for the E lobe. Given these spectral parameters and the narrow band width of the IPC, the mean energy of detected

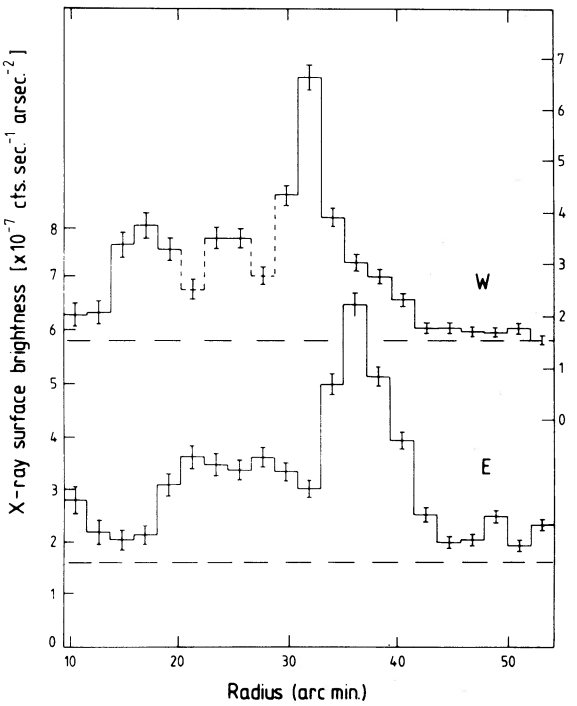

FIG. 2.—Radial distribution of X-ray surface brightness in the lobes. The value in each histogram bin is the average surface brightness in annuli of width 64″ in the position angle range $90° < \theta < 106°$ (E lobe), and $270° < \theta < 286°$ (W lobe). Estimated background levels are indicated by the dashed lines. The distributions are not shown inside $R \approx 10'$ since at smaller radii they are dominated by the wings of the SS 433 point source profile.

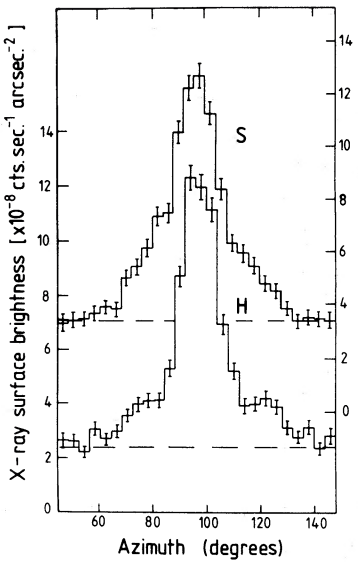

FIG. 3.—Azimuthal distribution of X-ray surface brightness in the E lobe. The value in each histogram bin is the average surface brightness in sectors of width 4° between radii $R \approx 10'$ and 54′ from SS 433. Estimated background levels are indicated by the dashed lines. The labels "S" and "H" refer to soft and hard energy ranges. S: ~ 0.4–1.0 keV; H: ~ 1.0–2.5 keV. The corresponding profiles for the W lobe (not shown) are very similar.

TABLE 2

DERIVED PARAMETERS FOR SS 433 AND LOBES

Object	Intensity (IPC counts s^{-1})	Luminosity[a] (ergs s^{-1})	Position R.A. Decl.	Radial Distance (arcmin)	Dimensions[b]
SS 433	0.95	$(1.7–8.1)\times10^{35}$	$19^h09^m20^s$	0.0	< 1′
(= V1343 Aql)	(variable)	4.3×10^{35}	+4°52′16″		
E lobe.....	0.18	5.8×10^{34}	...	...	R(in) < 15′ R(out) ~ 42′ R(max) ~ 35′ θ(FWHM) = 16° ± 2° θ(axis) = 98° ± 2°
W lobe	0.15	6.0×10^{34}	...	...	R(in) < 15′ R(out) ~ 44′ R(max) ~ 33′ θ(FWHM) = 14° ± 2° θ(axis) = 280° ± 2°
Peak emission, E lobe	0.035	1.0×10^{34}	19 11 40 +4 51 50	35.5 ± 1.0	~ 4′ × 5′
Peak emission, W lobe ...	0.025	1.0×10^{34}	19 07 10 +4 58 40	32.0 ± 1.0	~ 5′ × 5′

[a] Luminosities are calculated for $d = 5.5$ kpc and assumed spectra discussed in text. The upper value for SS 433 gives the luminosity in 1–10 keV band (from MPC results—Grindlay *et al.* 1983). All other values give luminosity in 0.5–4.5 keV band (from IPC results).

[b] R(in) = inner radius of lobe; R(out) = outer radius of lobe; R(max) = radius of peak in radial profile; θ(FWHM) = FWHM angular width of lobe; θ(axis) = position angle of axis of lobe.

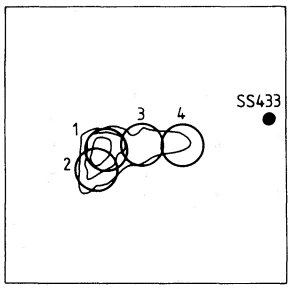

FIG. 4.—Positions of the four regions for which spectral analysis was performed shown on a schematic version of the E lobe X-ray map.

photons is close to 1.5 keV, justifying the choice of energy for the telescope vignetting correction applied to the data shown in Figure 1.

The total count rates observed from the E and W lobes (and smaller regions at the emission peaks) are also quoted in Table 2, together with their intrinsic luminosities calculated for a thermal spectrum with $kT = 2$ keV and $N_H = 10^{22}$ cm^{-2} and assuming a distance of 5.5 kpc. The integrated luminosity from each lobe is of the order 10% of that from SS 433 itself.

IV. INTERPRETATION

There can be little doubt that the emission from the X-ray lobes originates in the interaction between the jets ejected from SS 433 and the surrounding medium at large distances from the central object. The main evidence for this is the fact that the X-ray lobes (on scales of tens of arc minutes) lie at the same position angle as the arc second radio structure surrounding SS 433 itself. (We are also struck by the similarity of the X-ray lobe morphology to that of many extragalactic double radio sources whose radio lobes are commonly assumed to be formed by centrally ejected jets.) This conclusion clearly implies that the jets traverse large distances in the ISM without major perturbation, and that the kinematic parameters do not change rapidly, since the X-ray lobe morphology is at least crudely consistent with the present jet geometry.

Figure 5 shows a composite of the IPC X-ray map with the 2.7 GHz radio map of W50 by Downes, Pauls, and Salter (1981). Also shown are the positions of the faint optical H-alpha filaments discovered independently by van den Bergh (1979) and Zealey, Dopita, and Malin (1980). It is immediately striking that the lobes lie along the same axis as that defined by the E-W elongation of the W50 radio shell (thus strengthening the physical association between W50 and SS 433), and that the peak X-ray emission of both E and W lobes lies close (within ~ 5′) to the H-alpha filamentary structure. The undisturbed, approximately circular arcs of the radio shell N and S of SS 433 lie at a mean radius of ~ 30′. The X-ray emission peaks of both lobes lie at a similar radius approximately E and W of SS 433.

Indirect estimates can be made of other physical parameters of the ejected jets relevant to the interpretation of the X-ray lobes (e.g., Begelman *et al.* 1980; Milgrom 1981 and references therein). Consideration of the line widths of the "moving lines" implies initial jet collimation to ~ 5°; thus, we can imagine the jets to be

TABLE 3

IPC SPECTRAL RESULTS

	THERMAL[a]		POWER LAW[b]	
REGION	Best fit kT (keV)	90% confidence interval (keV)	Best fit alpha	90% confidence interval
1	1.5	1.0	4.0	3.3
		2.0		4.2
2	1.5	1.0	4.0	3.2
		2.0		4.8
3	2.0	1.4	3.0	2.3
		> 4.0		3.7
4	4.0	2.0	2.0	< 1.3
		> 4.0		3.0

NOTE.— The values of kT and alpha quoted correspond to single parameter fits including an absorption term $\exp[-\sigma(E)N_H]$ with N_H fixed at 10^{22} cm^{-2}. 90% confidence limits are evaluated as $\chi^2_{min} + 2.7$ (e.g., Lampton, Margon, and Bowyer 1976). Uncertainties in the precise background spectrum and detector gain introduce *additional* systematic errors whose magnitude we estimate to be $\leq 50\%$ of statistical errors quoted.

[a] Thermal spectrum for an optically thin plasma with cosmic abundances following Raymond and Smith (1977). Use of a single bremsstrahlung spectrum would give systematically lower values of kT.

[b] Power law spectrum of the form: $N(E) = AE^{-\alpha}$.

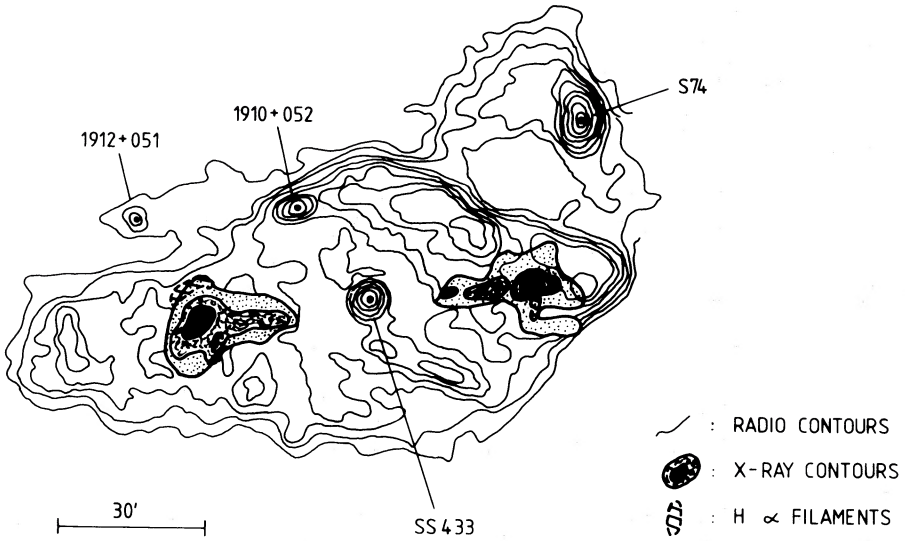

FIG. 5.—Composite X-ray and radio map of the SS 433/W50 region. The radio map is based on the 2.7 GHz map of Downes, Pauls, and Salter (1981) which has a half-power beamwidth of 4'.4. Note that S74, 1910+052 and 1912+051 are not believed to be associated with W50. The X-ray map is a simplified version of Fig. 1. Also shown are the positions of the H-alpha optical filaments after Zealey, Dopita, and Malin (1980).

initially confined to a thin shell on the surface of a cone with half-angle 20°. Estimates of the kinetic luminosity of the jets, again inferred from the emission-line spectrum, range from 10^{36} to 10^{42} ergs s^{-1} (corresponding to mass flow rates in the jets of 5×10^{-10} to 5×10^{-4} $M_\odot$ yr^{-1}), with most authors preferring estimates at the top end of this range.

Here we discuss two alternative explanations for the origin of the X-ray emission from the lobes: thermal emission from a hot plasma ($T\sim10^7$ K), or synchrotron emission from highly relativistic particles in the ambient magnetic field. We stress that we cannot distinguish between these mechanisms observationally since the IPC data are consistent with both thermal and power law spectral forms.

a) Thermal X-Ray Emission from the Lobes

The emission region in each lobe, assuming the lobes have a conical geometry, has an estimated volume $V\approx 6\times10^{59}$ cm^3 for $d=5.5$ kpc. Using the emissivity of a thermal plasma with $kT=2$ keV, the number density required to give the lobe luminosity is $n_e\sim0.1$ cm^{-3}, providing the medium is not clumpy. The cooling time for this plasma is long ($\sim3\times10^8$ yr), and the total energy content for both lobes is $E_{\rm th}\approx1.2\times10^{51}$ ergs. If this thermal energy is supplied by the jets over a timescale T_3 (where T_3 is in units of 10^3 years), the mean energy supply rate must have been $L_b\approx4\times10^{40}\,\varepsilon^{-1}\,T_3^{-1}$ ergs s^{-1}, where ε is the efficiency with which the jet kinetic energy is used to heat the plasma. Assuming that W50 is less than $\sim10^5$ yr old (i.e., $T_3\lesssim100$), the thermal interpretation constrains the kinetic luminosity of the jets to be $L_b\gtrsim4\times10^{38}\,\varepsilon^{-1}$ ergs s^{-1}. A shorter duration of the beaming process requires proportionately more energy in the jets. The lower limit to the beaming duration is the travel time to the edge of the remnant at $0.26c$, i.e. $\sim10^3$ yr, giving $\sim10^{41}$ ergs s^{-1} as an upper limit to the kinetic luminosity of the jets—an order of magnitude less than that inferred from the emission line spectrum by Begelman *et al.* (1981). The energy requirements of the thermal plasma thus do not exceed the independent estimates of the jet kinetic luminosity unless $\varepsilon\ll1$.

Since for thermal emission the emissivity of an isothermal plasma is proportional to n_e^2, the radial surface brightness profile of the lobes can be used to infer the density profile in the lobes. Taking into account the assumed conical geometry of the lobes, projection effects, and interstellar absorption, we have used the average of the E and W lobe profiles (Fig. 2) to determine the radial density distribution in the lobes. The derived number densities range from $n_e\sim0.7$ cm^{-3} at the emission peak at $R\approx35'$ from SS 433, to $n_e\sim0.16$ cm^{-3} for the faint emission plateau at $R>45'$.

These are based on the assumption of constant density within individual emitting regions. Unresolved structure or clumping of hot gas will raise the estimate of n_e, lower the total mass of emitting gas, and lower the energy required. Thus our calculation gives upper limits to mass and energy.

The implied density enhancement by a factor ~4 at $R\approx35'$ strongly suggests the presence of a shell at this radius. Indeed, a natural interpretation of the X-ray results is that the shell of W50, evident N and S of SS 433 in the radio maps at a radius of $\sim30'$ (~50 pc), also exists to the E and W of SS 433 at a slightly larger

radius (i.e. $\sim 35' \approx 55$ pc). (This is also suggested by the presence of the optical filaments.) The fact that the parts of the SNR shell not heated by the jets are not detected by the IPC can be explained if the shell is cool, since the effective attenuation by interstellar absorption in the IPC band is much greater for a low temperature plasma than for one with $T > 10^7$ K. The nondetection of most of the SNR shell then implies $T_s \lesssim 2 \times 10^6$ K; combining this with a shell radius ~ 55 pc in an adiabatic Sedov solution gives an age for W50 of $\gtrsim 50{,}000$ yr, and initial energy, assuming the density estimates from the lobe emission are applicable to the whole shell, of $\lesssim 7 \times 10^{51}$ ergs. These estimates are necessarily crude, especially since the shell radius along the axis of the lobes is $\sim 10\%$ greater, indicating that the jets have affected the dynamics of the shell.

Interpretation of the lobe emission as thermal requires that there be a reasonably efficient means for the jets to heat the medium to temperatures $\gtrsim 10^7$ K. A likely mechanism involves heating by shocks propagating outwards into the medium from the surface of the cone to which the jets are initially confined. Although the thermal interpretation of the lobe emission seems to be reasonably successful, we have no straightforward explanation for the detailed shape of the observed azimuthal profile of the lobes (i.e., Fig. 3), given that the jets are initially confined to the surface of a cone with half-angle $\sim 20°$. Shocks propagating both inward and outward from the surface of a cone would presumably give a center-brightened emission profile with broad, faint wings, but it is not clear that such a heating mechanism would reproduce the strongly enhanced core to the profile. Indeed, because we assume the medium is shock heated, the inference that there is hot plasma on the axis of the cone implies time scales for jet heating long enough ($\gtrsim 10^4$ yr) for the shocks to propagate inward at velocities of the order of the sound speed (~ 300 km s^{-1}) in the plasma.

b) Synchrotron X-Ray Emission from the Lobes

Synchrotron emission from relativistic particles in the lobes is a possible alternative to the thermal interpretation. Assuming equipartition between energy in relativistic electrons and in the magnetic field, the observed X-ray luminosity, together with the lobe volume of $\sim 6 \times 10^{59}$ cm^3 (see § IV*a*), yield an estimated magnetic field strength $B \sim 4 \times 10^{-6}$ gauss, and a total energy content in relativistic electrons and magnetic field of $\sim 10^{48}$ ergs. If this energy is supplied by the jets over a timescale T_3 yr, the mean energy supply rate must have been $L_b \approx 3 \times 10^{37}\ \varepsilon^{-1} T_3^{-1}$ ergs s^{-1}, three orders of magnitude lower than is required in the thermal interpretation. The electrons giving the X-ray emission have energies $\sim 6 \times 10^4$ GeV and radiative lifetimes of $\sim 10^4$ yr. Since inverse Compton losses are also important at this energy, this lifetime is actually an upper limit.

At radio wavelengths the interior of W50 has a strong nonthermal polarized flux which is almost certainly synchrotron in origin (Downes, Pauls, and Salter 1981). Since radio maps (e.g., Fig. 5) show no detailed correlation with the X-ray lobes, the synchrotron interpretation requires an *additional* population of particles in the lobes. From the Downes *et al.* maps, we derive an upper limit to the radio flux at 2.7 GHz correlated with the X-ray lobes of $S_{2.7} \lesssim 2$ Jy. Combining this limit with the observed X-ray flux constrains the power law spectral index α connecting the X-ray and radio parts of the assumed synchrotron spectrum to be $\alpha \lesssim 0.7$ ($S_\nu \propto \nu^{-\alpha}$).

The bulk of the X-ray emission from the lobes is concentrated in the region bounded by the surface of the cone defined by the jets and, at the ends, by part of the SNR shell. Since the energy density within the SNR shell is $\sim 10^{-10}$ ergs cm^{-3}, and that within the relativistic particle jets is probably about the same, there is no problem in confining the synchrotron lobes with an energy density $\sim 10^{-12}$ ergs cm^{-3}. Complete confinement is clearly not taking place, since significant X-ray emission is seen well outside the region delimited by the cones (cf. Fig. 3).

The high energy electrons required for synchrotron X-ray emission are plausibly generated by the Fermi process in which particle acceleration takes place in the region between the SNR shell and the jets by collisions with blobs of material in the jets. (The fact that the jets are "blobby" is clearly indicated in the detailed emission line profiles, e.g., Grandi and Stone 1982.) Each collision gives an average energy gain $\Delta E/E \approx 0.25$ ($= v/c$). Thus for electrons with initial energies ~ 5 GeV (i.e., those producing the radio synchrotron emission throughout the remnant), only ~ 40 collisions are needed to increase their energy by the factor $\sim 10^4$ required. The average time between collisions, if the particles are to reach the required energies on their radiative time scale, is $\lesssim 250$ yr. Unless the field is ordered, the electrons are expected to diffuse at the Alfvén velocity of ~ 100 km s^{-1}. Thus the electrons are not expected to travel the length of an X-ray emitting lobe during their lifetime, and this mechanism requires that the jets spread to fill the observed X-ray lobes and that they retain relativistic velocity throughout the length of the lobe.

In contrast with the thermal interpretation, the synchrotron explanation of the lobe emission does not allow an obvious understanding of the radial and azimuthal profiles of the lobes. However, since the synchrotron luminosity scales as E^2B^2, interpretation of these profiles could clearly invoke either an enhanced magnetic field or enhanced particle energies (or both) in the regions which show higher X-ray emission.

V. CONCLUSION

The shell of W50, as delineated by the radio source in the N and S, and by the optical filaments and X-ray

emission peaks in the E and W, appears to be approximately spherical, implying isotropic deposition of energy within the ISM. The size and estimated temperature of this shell are compatible with a SN releasing $\sim 10^{51}$ ergs into an ISM with density ~ 0.1 cm^{-3} and an age $\sim 10^5$ yr, although, at 5.5 kpc, W50 is somewhat larger than other cataloged "old" SNR. This may result from additional deposition of energy from SS 433 throughout the volume making W50 larger or brighter than remnants of similar age. Distortion of this shell by directed energy from SS 433 has been appreciable over only $\sim 20\%$ of the surface (assuming prolate geometry). The energy deposited within the shell by the jets is therefore, from the morphology of W50, an appreciable fraction of the original energy release, but not enough to eradicate the basic form of the shell. (Note similar arguments in Zealey, Dopita, and Malin 1980.) Furthermore, since there is no sign of energy deposited outside the edge of W50, the jets must deposit all their energy within the remnant.

The thermal emission model for the X-ray lobes fits this concept nicely. The lobes show regions containing $\sim 10^{51}$ ergs concentrated in directions exactly inside the radio ansae. The pressure of the hot plasma (~ 0.1 cm^{-3}, 2×10^7 K) is comparable to, or greater than, that of the material in the SNR shell (~ 1 cm^{-3}, $\sim 10^6$ K). In contrast, the pressure within the lobes in the synchrotron interpretation is ~ 100 times smaller, making it inconsistent with the apparent penetration of the SNR shell by the lobes to form the ansae. We therefore favor the thermal interpretation.

The lobes are high pressure regions where energy deposited by the jets has been concentrated prior to penetrating the SNR shell. The jets, consisting of blobs of high energy particles and magnetic field, originally form a hollow cone which envelops the X-ray lobes at small radii, probably blending into them toward the rim of the remnant, although the exact geometry of the jets is unknown (except close to SS 433). The jets probably confine the X-ray emitting plasma at the apex of the cone and restrict its expansion at larger radii, possibly providing an explanation for the center-brightened appearance of the lobes. Little X-ray emission is observed within ~ 15 pc of SS 433, presumably as a result of a much lower ambient density there (consistent with the evolution of a remnant following the adiabatic Sedov solution). This effect may also have been enhanced by the jets sweeping clear a channel close to SS 433. The exact mechanism by which the jets deposit energy in the hot plasma is not understood.

The X-ray lobes, the ansae, and the energetics are all consistent with (but do not require) a SN origin of W50 with subsequent modifications of the morphology by directed energy from SS 433. The morphology of the lobes of W50 is consistent with the jet geometry in the kinematic model, and, with steady beaming over the life of the SNR, the precessing jets can supply the directed energy, a large fraction of which is observable in the X-ray lobes.

We acknowledge several stimulating discussions with M. Begelman and thank many colleagues at both Leicester and CfA for advice and assistance. M. G. W. thanks the High Energy Astrophysics Division of CfA for their hospitality while some of this work was carried out. M. G. W. and R. W. were supported by the UK SERC, and F. D. S. and J. G. by NASA contract NAS 8-30751.

REFERENCES

Abell, G. O., and Margon, B. 1979, *Nature*, **279**, 701.
Begelman, M. C., Sarazin, C. L., Hatchett, S. P., McKee, C. F., and Arons, J. 1980, *Ap. J.*, **238**, 722.
Clark, D. H., Caswell, J. L., and Green, A. J. 1975, *Australian J. Phys. Ap. Suppl.*, **37**, 1.
Crampton, D., Cowley, A. P., and Hutchings, J. B. 1980, *Ap. J. (Letters)*, **235**, L131.
Downes, A. J. B., Pauls, T., and Salter, C. J. 1981, *Astr. Ap.*, **103**, 277.
Geldzahler, B. J., Pauls, T., and Salter, C. J. 1980, *Astr. Ap.*, **84**, 237.
Giacconi, R., *et al.* 1979, *Ap. J.*, **230**, 540.
Gorenstein, P., Harnden, F. R., and Fabricant, D. G. 1981, *IEEE Trans.*, **NS-28**, 826.
Grandi, S. A., and Stone, R. P. S. 1982, *Pub. A.S.P.*, **94**, 80.
Grindlay, J. E., Band, D., Seward, F. D., Leahey, D., Weisskopf, M. and Marshall, F. E. 1983, *Ap. J.*, submitted.
Hjellming, R. M., and Johnston, K. J. 1981, *Ap. J. (Letters)*, **246**, L141.
Lampton, M., Margon, B., and Bowyer, S. 1976, *Ap. J.*, **208**, 177.
Margon, B. 1981, in Proc. 10th Texas Symp. Relativistic Astrophysics, *Ann. NY Acad. Sci*, in press.
_____. 1982, in *Accretion Driven Stellar X-Ray Sources*, ed. W. H. G. Lewin and E. P. J. van den Heuvel (Cambridge: Cambridge University Press), in press.
Margon, B., Ford, H. C., Katz, J. I., Kwitter, K. B., Ulrich, R. K., Stone, R. P. S., and Klemola, A. 1979, *Ap. J. (Letters)*, **230**, L141.
Milgrom, M. 1981, *Vistas in Astronomy*, **25**, 141.
Raymond, J. C., and Smith, B. W. 1977, *Ap. J. Suppl.*, **35**, 419.
Seward, F. D., Grindlay, J. E., Seaquist, E., and Gilmore, W. 1980, *Nature*, **287**, 806.
van den Bergh, S. 1980, *Ap. J. (Letters)*, **236**, L23.
Velusamy, T., and Kundu, M. R. 1974, *Astr. Ap.*, **32**, 375.
Zealey, W. J., Dopita, M. A., and Malin, D. F. 1980, *M.N.R.A.S.*, **192**, 731.

JONATHAN E. GRINDLAY and FREDERICK D. SEWARD: Harvard-Smithsonian Center for Astrophysics, 60 Garden Street, Cambridge, MA 02139

MICHAEL G. WATSON and R. WILLINGALE: X-Ray Astronomy Group, Physics Department, University of Leicester, University Road, Leicester LE1 7RH, England